

Spirooxindol-1,3-oxazine Alkaloids: Highly Potent and Selective Antitumor Agents Evolved from Iterative Structure Optimization

Annika Eichhorst,^[a] Malte Gallhof,^[b] Alice Voss,^[b] Anett Sekora,^[a] Leon Eggers,^[a] Le Thi Huyen,^[d] Christian Junghanss,^[a] Hugo Murua Escobar^{+, * [a]} and Malte Brasholz^{+, * [b, c]}

Spirooxindole-1,3-oxazines are a small and structurally unique class of spirooxindole alkaloids. To date, only four of these compounds have been isolated from natural sources, and their biological properties remained unknown thus far. Dioxyreserpine is a synthetic spirooxindole-1,3-oxazine, that can readily be prepared from the *Rauvolfia* alkaloid (–)-reserpine by catalytic photooxygenation. While dioxyreserpine itself was now identi-

fied as a moderately effective antitumoral agent, structurally modified analogs of it emerged as a new class of highly potent and selective growth inhibitors of various human cancers, including pancreatic cancers. Systematic structural optimization ultimately led to an inhibitor displaying low-micromolar IC₅₀-values against six cancer cell lines as well as selective apoptosis induction *in vitro*.

Introduction

Small molecules, together with biologicals, form the foundation of targeted therapies in oncology and offer the possibility of establishing therapy protocols tailored to the individual patient.^[1] Despite the successful introduction of various small molecules into different oncological therapy concepts, a significant proportion of patients show a non-response or a recurrence of the disease.^[2] A possible reason for this problem is with high probability the different genetic background of

oncological diseases of the same entity (tumor heterogeneity) at the beginning of therapy, as well as the accumulation of genetic changes of the initial neoplasia during therapy itself.^[3] Many nitrogen-containing heterocycles are considered privileged structural motifs, and some drugs derived from them are also used therapeutically in oncology.^[4]

Naturally occurring indole alkaloids offer a plethora of useful biological properties, and since ancient times traditional medicine has made use of them.^[5] Spirooxindoles constitute a structurally intriguing and medicinally highly valuable class of indole alkaloids. Roughly 75% of all known spirooxindoles possess the most common core structure, the spiro[pyrrolidin-3,3'-oxindole] motif **A** (Scheme 1a).^[6] A large number of these compounds display analgesic, antibiotic and antitumoral activities.^[7] Regarding the latter, the natural product mitraphylline (**1**), active against leukemia, sarcoma, and breast cancer,^[8] as well as the synthetic inhibitor of the P53-MDM2 interaction, MI-888 (**2**)^[9] are prominent examples.

A small and quite peculiar class of spirooxindoles is made up of compounds that possess a spiro[(1,3)-oxazin-3,6'-oxindole] core structure **B** (Scheme 1b). By 2022, the isolation of only four natural products of this genus had been reported, all of which originate from South East Asian shrubs and flowering plants: Mitraversifoline **3**,^[10] uncarialine D **4**,^[11] nauclealomid A **5**^[12] and melodinoxanine **6**.^[13] The biosynthetic pathways leading to these alkaloids remain to be elucidated as well as their potential medicinal uses. However we can anticipate the isolation of more representatives of this interesting compound family.

A purely synthetic and thus readily available spirooxindole-1,3-oxazine is dioxyreserpine (**8**), that can be prepared in larger quantities by the catalytic photooxygenation^[14,15] of the *Rauvolfia* alkaloid reserpine (**7**), which is sold commercially at relatively low cost (Scheme 1c). Dioxyreserpine (**8**) equals the polycyclic natural products **3–6** in their level of molecular complexity, and also its absolute configuration at the C-3 and C-7 stereocenters

[a] A. Eichhorst, A. Sekora, L. Eggers, Prof. Dr. C. Junghanss, PD Dr. H. Murua Escobar⁺
Department of Internal Medicine
Medical Clinic III
Clinic for Hematology, Oncology and Palliative Care
University Medical Center Rostock
Ernst-Heydemann-Strasse 6,
18057 Rostock (Germany)
E-mail: hugo.murua.escobar@med.uni-rostock.de

[b] M. Gallhof, A. Voss, Prof. Dr. M. Brasholz⁺
Institute of Chemistry – Organic Chemistry
University of Rostock
Albert-Einstein-Str. 3 A, 18059
Rostock (Germany)
E-mail: malte.brasholz@uni-rostock.de

[c] Prof. Dr. M. Brasholz⁺
Leibniz Institute for Catalysis at the University of Rostock
Albert-Einstein-Str. 29 A, 18059
Rostock (Germany)

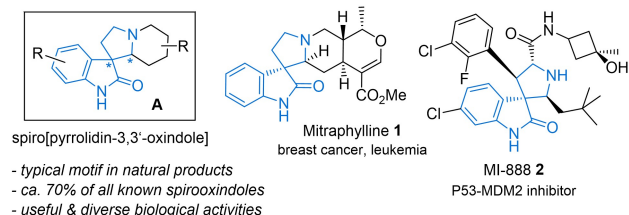
[d] Dr. L. T. Huyen
Vietnam National University
Hanoi University of Science
Hanoi, 334 Nguyen Trai, Thanh Xuan,
Hanoi (Vietnam)

[†] These authors contributed equally to this work.

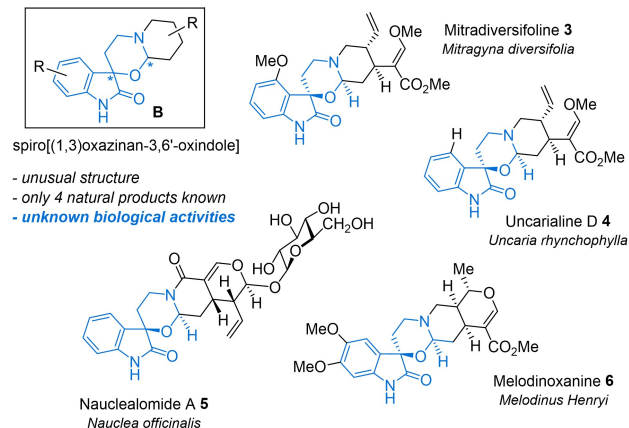
Supporting information for this article is available on the WWW under <https://doi.org/10.1002/cmdc.202200162>

© 2022 The Authors. ChemMedChem published by Wiley-VCH GmbH. This is an open access article under the terms of the Creative Commons Attribution Non-Commercial NoDerivs License, which permits use and distribution in any medium, provided the original work is properly cited, the use is non-commercial and no modifications or adaptations are made.

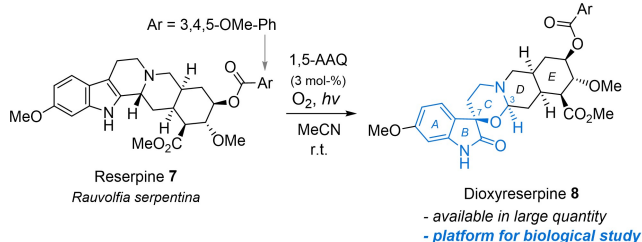
a) Typical structure of oxindole alkaloids



b) Spirooxindole-1,3-oxazines



c) Photooxygenation of (-)-reserpine



Scheme 1. a) Structures of spiro[pyrrolidin-3,3'-oxindole] alkaloids. b) Natural spiro[(1,3)oxazinan-3,6'-oxindole] alkaloids. c) Catalytic photooxygenation of reserpine (7) to dioxyreserpine (8). 1,5-AAQ = 1,5-Diaminoanthraquinone.

of the 1,3-oxazine ring is identical. Its *cis*-fused *D* and *E* rings, a structural specialty that gives the whole molecule a strong curvature, are also present in melodinoxanine 6. These features make dioxyreserpine (8) an ideal starting point for a biological study that, if it would establish any desirable medicinal proper-

ties, would suggest that natural products of the spirooxindole-1,3-oxazine structure B are of general medicinal interest.

Results and Discussion

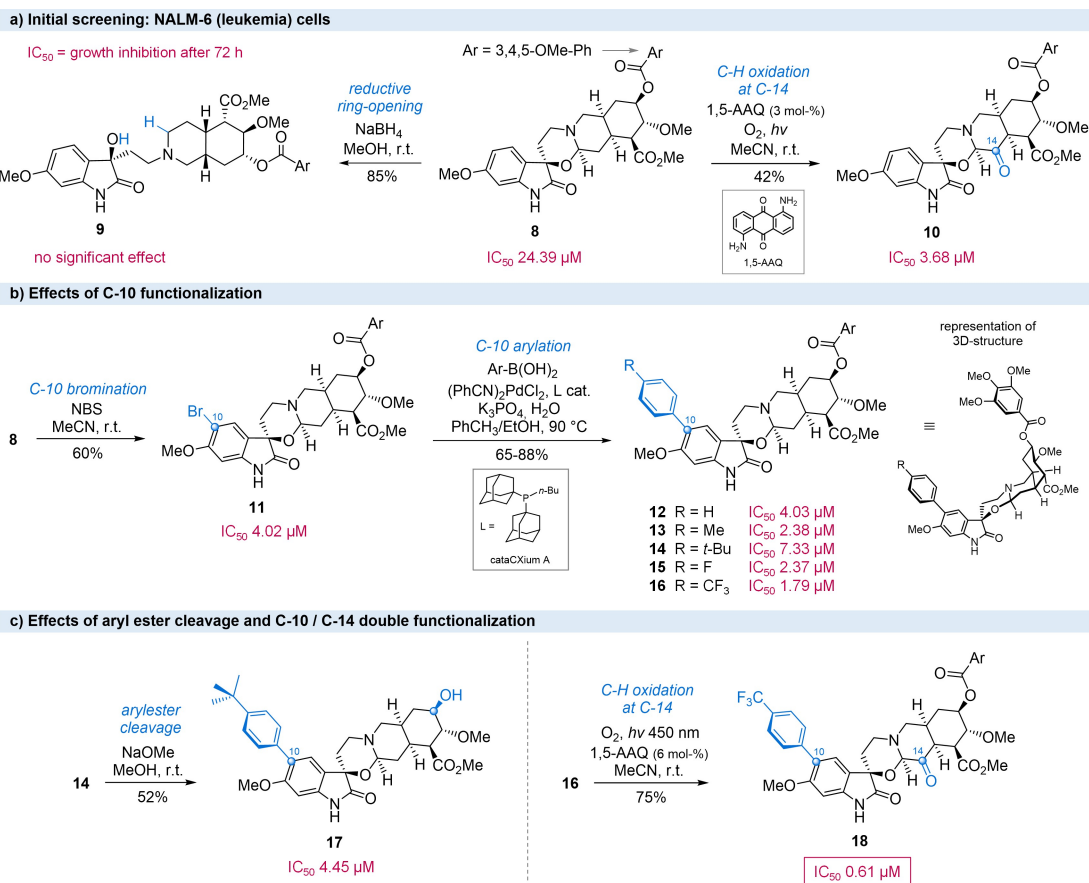
Our investigations began with an initial screening of dioxyreserpine (8) for its growth inhibitory activity against six human cancer cell lines, i.e. the B-ALL cell lines RS4;11 and NALM-6, the lymphoma cell lines SU-DHL-4 and SUP-T1, and the pancreatic carcinoma cell lines MIA-PaCa-2 and Capan-1. After 72 h of incubation, a cell count was carried out for the haematological cell lines, while for the solid cell lines, the cell mass was determined using crystal violet staining. The metabolic activity was also quantified with the WST-1 assay (see further below). Of all cell lines, NALM-6 appeared to be most responsive to incubation with dioxyreserpine (8), showing a moderate growth inhibition and an IC_{50} of $24.39 \pm 19.26 \mu\text{M}$ after 72 h (Table 1, 1st row). Hence we continued our investigation with NALM-6 and employed structurally modified derivatives of dioxyreserpine (8) as shown in Scheme 2. The reductive ring-opening of 8 with NaBH_4 leads to compound 9,^[14] that showed no significant effects, clearly confirming that the spirooxindole-1,3-oxazine structure is essential for activity. On the other hand, the C-14-oxidized derivative trioxyreserpine (10), which is accessible from 8 by another catalytic photooxygenation,^[14] showed a markedly increased growth inhibition, with a superior IC_{50} of $3.68 \pm 1.46 \mu\text{M}$ (Scheme 2a).

The subsequent course of the investigation was decisively altered by the discovery that functionalization of dioxyreserpine (8) in the C-10 position had a pronounced positive effect (Scheme 2b). Electrophilic bromination of 8 leads to C-10 bromide 11,^[14] that showed strong growth inhibition with an IC_{50} of $4.02 \pm 1.61 \mu\text{M}$. Hence we hypothesized that the introduction of other hydrophobic groups in this position would be beneficial. Bromide 11 undergoes clean Suzuki arylations with arylboronic acids when using $(\text{PhCN})_2\text{PdCl}_2$ as the Pd(0) precursor, in combination with the CataCXium® A ligand.^[16] The C-10 biaryl derivatives 12–16 are obtained in 64–88% yield under these conditions, and pleasingly, they show strongly improved inhibitory activity compared to the parent dioxyreserpine (8), with IC_{50} ranging from 4.03 ± 1.29 to $1.79 \pm$

Table 1. Collected IC_{50} values [μM] of compounds 8–18 for growth inhibition of six human carcinoma cell lines after 72 h incubation time.^[a]

Compound	SU-DHL-4	SUP-T1	NALM-6	RS4;11	MIA-PaCa-2	Capan-1
8	61.40 ± 16.26	74.47 ± 50.78	24.39 ± 19.26	n.c.	n.c.	n.c.
9	n.c.	n.c.	n.c.	63.73 ± 35.77	n.c.	n.c.
10	2.93 ± 0.66	2.85 ± 1.03	3.68 ± 1.46	2.97 ± 1.66	3.99 ± 0.30	23.01 ± 12.40
11	12.62 ± 7.15	19.24 ± 17.97	4.02 ± 1.61	10.25 ± 5.85	21.21 ± 2.42	88.14 ± 38.46
12	31.92 ± 14.60	n.c.	4.03 ± 1.29	10.23 ± 7.24	21.81 ± 12.85	61.92 ± 21.20
13	1.39 ± 0.07	4.72 ± 1.52	2.38 ± 0.10	3.71 ± 0.87	4.18 ± 1.32	22.15 ± 11.01
14	15.93 ± 6.00	n.c.	7.33 ± 3.31	21.26 ± 39.35	n.c.	n.c.
15	2.26 ± 0.33	7.01 ± 0.05	2.37 ± 1.16	3.52 ± 4.26	7.04 ± 1.99	28.91 ± 59.53
16	1.73 ± 0.17	3.64 ± 3.48	1.79 ± 0.62	1.95 ± 0.53	6.11 ± 2.07	n.c.
17	n.c.	n.c.	4.45 ± 0.47	n.c.	n.c.	n.c.
18	1.14 ± 0.20	1.62 ± 0.13	0.61 ± 0.38	0.32 ± 0.06	1.90 ± 0.88	4.21 ± 0.95

[a] Cell count was carried out for the haematological cell lines. For the solid cell lines, the cell mass was determined using crystal violet staining. n.c. = not calculable.



Scheme 2. Initial screening, structural variation and iterative optimization of the growth inhibition of NALM-6 leukemia cells. IC_{50} values determined after 72 h incubation.

0.62 μM . Up to this point, all compounds tested contained the hydrophobic 3,4,5-trimethoxyphenyl ester moiety attached to the C-18 hydroxyl group on the *E*-ring. As shown exemplary for compound 14, the saponification of the ester only has little influence on the growth inhibition of NALM-6, as IC_{50} decreased only slightly from $7.33 \pm 3.31 \mu\text{M}$ for compound 14 to $4.45 \pm 0.47 \mu\text{M}$ for compound 17. Other cell lines however responded more strongly to this structural change (Table 1, compare rows 7 and 10).

Based on our observations that introduction of a hydrophobic aromatic group at C-10 and the carbonyl group at C-14 both strongly improved activity, we reasoned that combining these two modifications potentially would lead to an even more potent inhibitor. Hence, 4-trifluoromethylphenyl-substituted compound 16, most active among the biaryls 12–16, was subjected to C-14 methylene oxidation. Gratifyingly, when the C–H oxidation is performed under the photooxygenation conditions developed previously for the oxidation of dioxyreserpine (8) to trioxyreserpine (10), compound 18 is isolated in a reproducibly high yield of 75%.

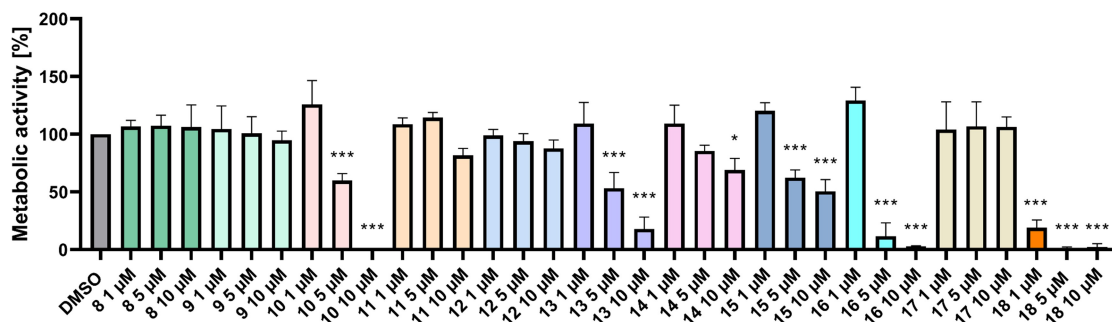
In the subsequent screening, the C-10, C-14 difunctionalized derivative, 10-(4-trifluoromethylphenyl)trioxyreserpine (18), emerged as a highly potent growth inhibitor of all six cell lines investigated (Table 1, last row). Its IC_{50} values significantly fall

below all of those of trioxyreserpine (10) and 4-trifluoromethylphenyl-substituted biaryl 16 for SU-DHL-4 ($1.14 \pm 0.20 \mu\text{M}$), SUP-T1 ($1.62 \pm 0.13 \mu\text{M}$), NALM-6 ($0.61 \pm 0.38 \mu\text{M}$) as well as RS4;11 which suddenly is the most sensitive cell line ($0.32 \pm 0.06 \mu\text{M}$) and MIA-PaCa-2 ($1.90 \pm 0.88 \mu\text{M}$). Of particular importance, of all compounds tested, compound 18 is the only one to effectively inhibit the pancreatic cancer cell line Capan-1, with an IC_{50} of $4.21 \pm 0.95 \mu\text{M}$; this represents a 90-fold increase in activity compared to dioxyreserpine (8), the starting point of the structure optimization.

Metabolic activity

The new spirooxindole derivatives were tested for their *in vitro* metabolism-modulating effects on lymphoma cell lines SU-DHL-4 and SUP-T1, the B-ALL cell lines NALM-6 and RS4;11 and moreover pancreatic cancer cell lines MIA-PaCa-2 and Capan-1, by using the WST-1 assay after 72 h of incubation (Figure 1a). Regarding the results of the WST-1 assay we could observe an extraordinary increase of the metabolism-modulating effect on all cell lines, due to the structural modification of the parent compound dioxyreserpine (8). For B-ALL cell line RS4;11 we identified compounds 10, 13, and 15–18 to have a significant

a) RS4;11 metabolic activity after 72 h incubation, WST-1 assay



b) Haemolytic activity of compounds 8-18 after 2 h incubation

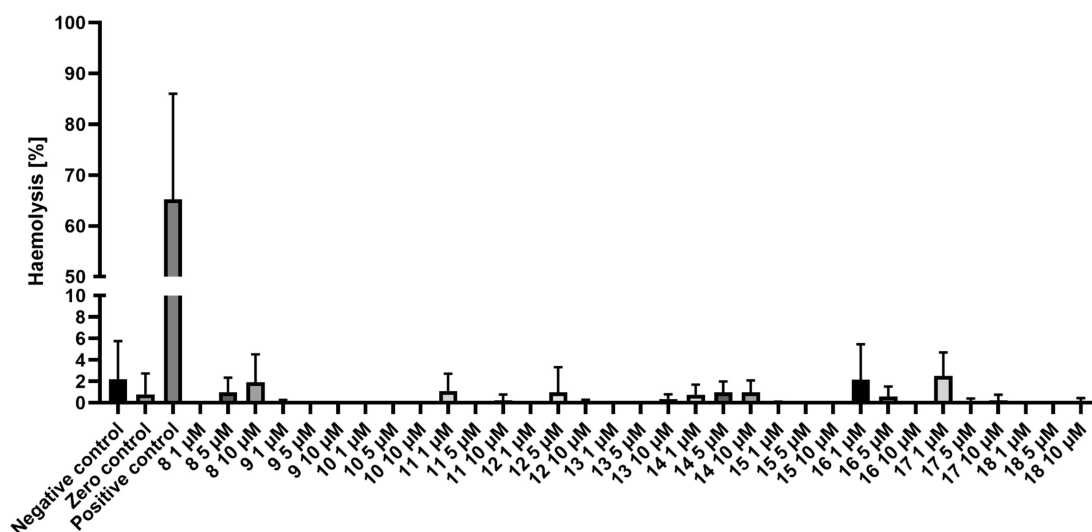


Figure 1. a) Results of WST-1 assay after 72 h of concentration-dependent spirooxindole exposure on B-ALL cell line RS4;11. Data are presented as mean \pm SD ($n \geq 3$). Statistical significance was calculated by one-way ANOVA. b) Haemolytic activity of spirooxindole derivatives after an incubation period of 2 h. Shown are means with \pm SD ($n \geq 3$).

reducing effect on metabolic activity (Figure 1b). Compound 18 showed the strongest effect for all tested concentrations. 1 μ M of compound 18 resulted in a reduction of metabolic activity to 19,04 % \pm 5,44 %, 5 μ M to 1,09 % \pm 1,06 %, respectively. Compounds 10 and 17 showed similar results for the highest concentration of 10 μ M.

Haemolysis

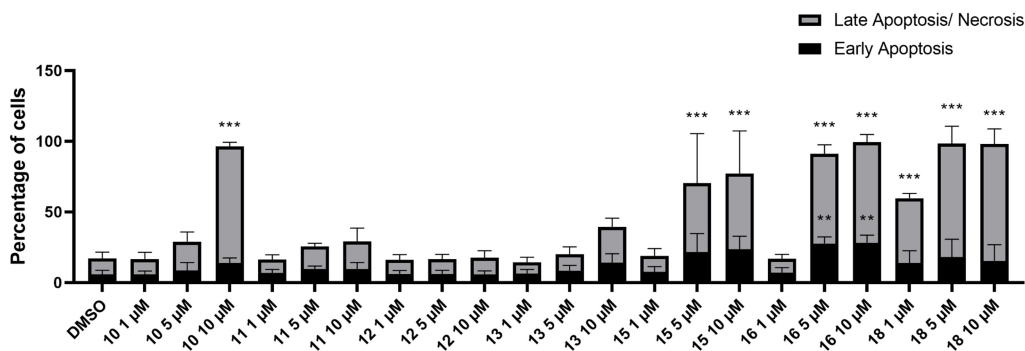
To preclude a potential haemolytic activity of the new spirooxindole derivatives, we measured the haemolysis of whole blood from three donors, 2 h after substance application (Figure 1b). None of the tested spirooxindoles showed a significant increase of haemolysis compared to negative control (only whole blood) or zero control (whole blood + PBS), which indicates the absence of erythrocyte toxicity.

Apoptosis induction and morphological characterization

Flow-cytometric analysis after Annexin-V FITC/PI double staining was used to observe a potential pro-apoptotic effect after 24, 48 and 72 h of the spirooxindole-1,3-oxazine derivatives (Figure 2a). The results indicate a significant increase of late apoptosis after all tested time points for the highest concentration of compound 10. Here the portion of late apoptotic cells increased from 9.82 % \pm 2.97 % in the control up to 82.71 % \pm 2.81 % after 72 h exposure. For compound 15 at concentrations of 5 μ M and 10 μ M we could also observe a significant increase of late apoptotic cells up to 48.70 % \pm 35.16 % and 53.68 \pm 30.18 % and early apoptosis from 5.07 % \pm 2.31 % in the control to 21.56 % \pm 13.11 % and 23.51 % \pm 9.33 % after 72 h, respectively. Incubation of RS4;11 cells with Compound 18 led to a significant increase of late apoptosis for all tested concentrations to 45.89 % \pm 2.78 %, 80.45 % \pm 10.00 % and 82.60 % \pm 8.80 % for the highest concentration of 10 μ M.

Microscopic analysis after May-Gruenwald-Giemsa staining revealed the presence of membrane blebs in case of com-

a) RS4;11 apoptosis induction after 72 h incubation



b) RS4;11 cell morphology after 72 h incubation with c = 10 µM of inhibitor

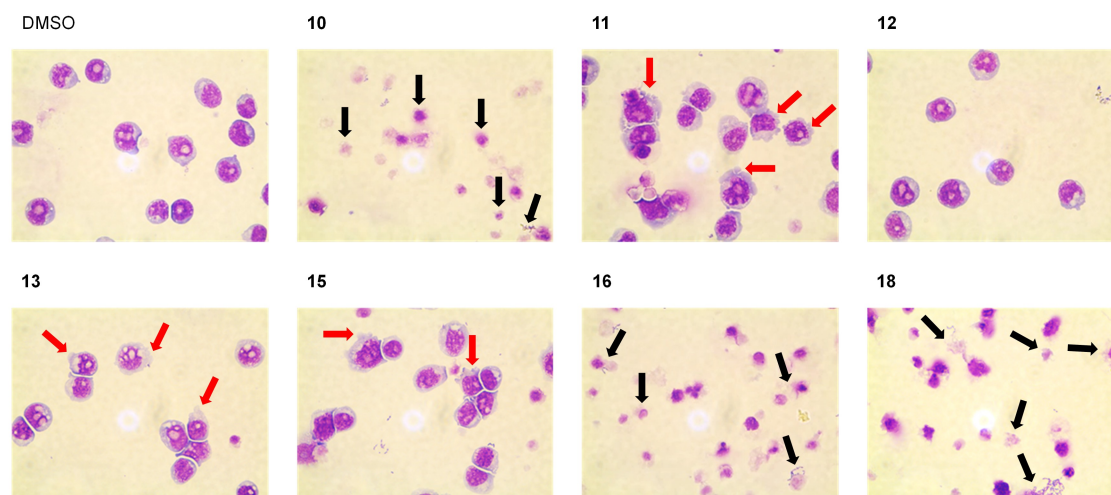


Figure 2. a) Apoptosis induction in RS4;11 cells after concentration-dependent spirooxindole exposure. Apoptosis induction was determined by using Annexin-V FITC/PI double staining after an incubation period of 72 h. Shown are means with \pm SD ($n \geq 3$). b) Morphological characterization of RS4;11 cells after exposure to 10 μ M of each compound for 72 h. DMSO was used as a control. The red arrows point to the membrane blebs and the black arrows to the cell detritus.

pounds 11, 13 and 15 (Figure 2b, red arrows). Morphological characterization of RS4;11 cells after exposure to 10 μ M of compounds 10, 16 and 18 showed the presence of detritus and cell debris (Figure 2b, black arrows), but no more intact and vital cells compared to DMSO control cells.

Cell-cycle analysis

In addition to the flow cytometric apoptosis measurements, the cell cycle was also analyzed after 48 h and 72 h. The results of the cell cycle analyzes for the B-ALL cell line RS4;11 after 72 h are shown below (Figure 3). The data were evaluated using the FlowJo™ software. For 10 μ M of compound 10, 5 μ M and 10 μ M of compound 13, 10 μ M of compound 15, as well as 5 μ M and 10 μ M of compound 16, no evaluation with the software could be carried out, since the cells are totally fragmented, so that cell cycle classification was not possible (Figure 3a).

Compared to the DMSO control, the application of compound 11 at a concentration of 5 μ M resulted in a significant reduction in the number of cells in the S phase. The proportion was reduced here from 40.73% \pm 7.46% in the DMSO control to 27.67% \pm 8.62%. At a concentration of 10 μ M, the proportion of the S phase decreased significantly to 17.83% \pm 5.28%. The proportion of the G1 phase also increased significantly from 45.13% \pm 4.48% in the DMSO control to 66.43% \pm 6.92%. At a concentration of 5 μ M, compound 10 showed a significant increase in the G1-phase population from 45.13% \pm 4.48% to 63.37% \pm 2.02% and an associated reduction in the S-phase population of 40.73% \pm 7.46% to 21.83% \pm 2.52%. Through the application of derivatives 10 and 11, a substance-induced G1 phase arrest could be observed in RS4;11 cells. Derivative 15 showed a significant increase in sub-G1 phase, confirming the induction of apoptosis and the results shown previously.

1 H, 6^s-H), 1.89 (q, $J=12.8$ Hz, 1 H, 19^b-H), 2.01–2.13 (m, 1 H, 19^b-H), 2.36–2.50 (m, 2 H, 6^b-H, 20-H), 2.53 (dd, $J=5.3, 10.5$ Hz, 1 H, 16-H), 2.83–2.95 (m, 2 H, 5^a-H, 21^a-H), 3.12 (dd, $J=2.5, 12.2$ Hz, 1 H, 21^b-H), 3.40 (m, 1 H, 5^b-H), 3.49–3.57 (m, 1 H, 15-H), 3.63 (s, 3 H, 33-H), 3.66 (s, 3 H, 34-H), 3.75 (s, 3 H, 35-H), 3.92 (s, 9 H, 30-H, 31-H, 32-H), 4.04 (dd, $J=9.3, 10.5$ Hz, 1 H, 17-H), 4.97 (ddd, $J=4.8, 9.3, 12.0$ Hz, 1 H, 18-H), 5.35 (s, 1 H, 3-H), 6.42 (s, 1 H, 12-H), 7.31 (s, 3 H, 9-H, 25-H, 29-H), 7.50 (s, 1 H, 1-H), 7.56 (d, $J=8.5$ Hz, 2 H, 37-H, 41-H), 7.61 (d, $J=8.5$ Hz, 2 H, 38-H, 40-H) ppm. ¹³C-NMR (125 MHz, CDCl₃): $\delta=31.3$ (C-6), 31.8 (C-19), 36.0 (C-20), 46.7 (C-16), 48.3 (C-5), 51.1 (C-15), 52.1 (C-34), 55.9 (C-21), 56.1 (C-35), 56.4 (C-30, C-32), 60.99 (C-33), 61.07 (C-31), 75.0 (C-7), 77.3 (C-17), 78.2 (C-18), 87.9 (C-3), 94.6 (C-12), 106.9 (C-25, C-29), 121.6 (C-8), 124.5 (q, $^1J_{CF}=272.1$ Hz, C-42), 125.0 (q, $^3J_{CF}=3.7$ Hz, C-38, C-40), 125.2 (C-24), 125.4 (C-10), 126.9 (C-9), 128.9 (q, $^2J_{CF}=32.7$ Hz, C-39), 129.8 (C-37, C-41), 141.7 (C-13), 141.8 (C-36), 142.5 (C-27), 153.1 (C-26, C-28), 158.5 (C-11), 165.6 (C-23), 171.4 (C-22), 177.5 (C-2), 201.1 (C-14) ppm. ¹⁹F-NMR (470 MHz, CDCl₃): $\delta=-62.39$ ppm. HRMS (ESI-TOF) m/z : calc. for C₄₀H₄₂F₃N₂O₁₂ [M+H]⁺: 799.2690, found 799.2690. IR: $\nu=3300, 2945, 2835, 1715, 1325, 1220, 1120, 1105, 725$ cm⁻¹.

Molecular and cell biology

Cell lines and cell culture methods. The human ALL cell lines NALM-6, RS4;11 (both B-ALL) and the human lymphoma cell lines SU-DHL-4 (B-cell) and SUP-T1 (T-cell) as well as the pancreatic cancer cell lines MIA-PaCa-2 and Capan-1 were purchased from DSMZ (Braunschweig, Germany). The cells were cultivated as recommended by the manufacturer protocol. All the cell lines were cultivated at 37 °C and 5 % CO₂ in the corresponding media with 10–15 % heat-inactivated FKS (Biochrom, Berlin, Germany) and 100 µg/ml penicillin and streptomycin (Biochrom, Berlin, Germany).

Drug exposure experiments. The suspension cell lines (3.3 × 10⁵ cells) and adherent cell lines were treated with each substance in three different concentrations (1 µM, 5 µM and 10 µM). Therefore the cells were cultured in the appropriate medium containing 0.1 % (v/v) DMSO as a control or dose ranges of the different derivatives as single substance for 24 h, 48 h and 72 h, depending on the experimental assay. After the incubation period, the effect on cell proliferation (trypan blue staining) or cell mass (crystal violet staining) in case of solid cells, metabolism (WST-1 assay), apoptosis/necrosis (annexin V/PI staining), cell cycle analysis, live cell imaging and morphology were determined. All experiments were performed at least in three biological replicates.

WST-1 assay. Haematological cell lines NALM-6, RS4;11, SU-DHL-4 and SUP-T1 were seeded in a 96-well plate at a density of 5 × 10⁴ cells per well in 150 µl media containing the substances or DMSO (0.1 % v/v) as a control. Pancreatic cancer cell lines MIA-PaCa-2 and Capan-1 were seeded at a density of 5 × 10³ cells and were allowed to attach overnight in the incubator (37 °C, 5 % CO₂). After attachment of cells, the media was removed and 150 µl of substance/DMSO containing media was added. All experiments were carried out in biological and technical replicates. After incubation period of 72 hours, 15 µl of WST-1 reagent was added to each well and the plates were again incubated for the next 3 h. The absorbance at 450 nm and a reference wavelength at 750 nm were determined using the GloMax-Multi Microplate Multimode Reader (Promega, Madison, WI, USA). For background control, 150 µl of the appropriate media containing 15 µl WST-1 was used.

Proliferation assay. To evaluate the impact of newly synthesized spirooxindoles, cell count was performed for the haematological cell lines NALM-6, RS4;11, SU-DHL-4 and SUP-T1. Therefore 5 × 10⁵ cells were seeded in 24-well plates and exposed to all substances (1 µM, 5 µM, 10 µM). DMSO (0.1 % v/v) exposed cells served as

control. After 72 h of incubation, the cells were harvested and washed with PBS. The number of viable cells were determined by cell count after trypan blue staining.

Crystal violet staining. In case of solid cancer cell lines MIA-PaCa-2 and Capan-1, crystal violet staining was carried out, to determine the cell mass after substance application. For both cell lines 5 × 10⁴ cells were seeded in 96-well-plates and let them adhere overnight. After adding the substances and 72 h of incubation, the supernatant was discarded and the cells were washed with 150 µl PBS. Thereafter 50 µl of crystal violet staining solution was added for 10 minutes. After two washing steps with 150 µl PBS, the cells were dried for 2 h. To detach the cells, 100 µl of 1 % SDS was used. The absorbance at 560 nm were determined using the GloMax-Multi Microplate Multimode Reader (Promega, Madison, WI, USA).

Haemolysis assay. Haemolytic activity of selected spirooxindole compounds was determined by haemoglobin release from whole blood cells. Shortly, whole blood of healthy donors ($n \geq 3$) was seeded in 96-well plates (round bottom) and incubated with 1 µM, 5 µM and 10 µM of each substance for 120 min. Positive control cells (=maximum lysis) were treated with 1 % Sodium Dodecyl Sulfate (SDS, Merck KGaA). Following the incubation period of 2 h, cell-free supernatants were transferred into a new 96-well plate (flat bottom) and absorption was measured on GloMax-Multi Microplate Multimode Reader (Promega, Madison, WI, USA) at 540 nm. Haemolytic activity was quantified according to the following formula: % haemolysis = $[(OD_{540\text{ nm sample}} - OD_{540\text{ nm buffer}}) / (OD_{540\text{ nm max}} - OD_{540\text{ nm buffer}})] \times 100$.

Morphological characterization. Morphological changes were determined by May-Gruenwald-Giemsa staining. Therefore the cells (0.5 × 10⁶) were seeded in a 24-well plate (flat bottom) and incubated with the compounds in concentration range of 1 µM to 10 µM for 24 h, 48 h and 72 h. After incubation period, 0.5 × 10⁴ cells were immobilized to cover slides with the cytospin 3 technology (Shandon, Frankfurt/Main, Germany). After staining, the morphological changes were analysed by microscopic analysis with EVOS[®] XL Core Imaging System (AMG, Washington, DC, USA).

Analysis of apoptosis. Determination of apoptosis induction was carried out by flow cytometric analysis using a FACS Calibur (BD Biosciences, Heidelberg, Germany). After incubation with each substance for 24 h, 48 h and 72 h in different concentrations (1 µM, 5 µM and 10 µM), cells were double stained with fluorescent dyes Annexin V-FITCS and propidium iodide. During apoptosis the membrane phospholipids were translocated to the cell surface and Annexin V binds to it. Propidium iodide is a DNA-intercalator, which binds to cellular nucleic acids of late apoptotic and necrotic cells with no intact cell membrane. The cells were harvested and washed twice with cold PBS (10 min, 180 g, 4 °C) and the pellet was resuspended in 100 µl Annexin Binding Buffer. 5 µl Annexin V FITCS were added to cell suspension and incubated for 15 min in the dark (RT). After incubation period, 400 µl Annexin Binding Buffer were added.

Cell-cycle analysis. Changes within the rates of cell cycle phases (G0/G1, S and G2/M) after 48 h and 72 h of incubation with each substance were examined by flow cytometric analysis using FACS Calibur (BD Bioscience, Heidelberg, Germany). After an RNase digest of ethanol fixed cells, cells were stained with the DNA intercalator propidium iodide. Emission signals are proportional to DNA mass. Signal peaks were identified for each phase due to the amount of DNA. Thereby G0/G1 phase cells has one set of paired chromosomes per cell, G2/M phase cells two sets of paired chromosomes per cell, prior to cell division and S-phase cells with variable DNA amount during DNA synthesis. Data analysis was carried out by using the FloJo[™] software (BD Bioscience, Heidelberg, Germany).

Statistical analysis. All values are constituted as mean \pm standard deviation. After testing for normal contribution, the differences between treated cells and control cells were evaluated using the one-way ANOVA. A p-value $< 0,05$ was set as statistically significant. IC₅₀ values were calculated according to the mathematical model (Prism 8.0.2, dose-response-inhibition vs. normalized response-variable slope).

Acknowledgements

Annika Eichhorst is grateful for a Ph.D. scholarship of the Landesgraduiertenförderung, University of Rostock, State of Mecklenburg-Vorpommern, Germany. Le Thi Huyen thanks the "RoHan" program between the University of Rostock and Vietnam National University - Hanoi University of Science for a research scholarship, which was funded by the German Academic Exchange Service (DAAD, project no. 57315854) and the Federal Ministry for Economic Cooperation and Development (BMZ) inside the framework "SDG Bilateral Graduate school program". We would further like to thank Michael Müller and Wendy Bergmann (Department of Core Facility for Cell Sorting and Cell Analysis, Rostock University Medical Center, Germany) for the possibility of Flow Cytometry device usage and technical support. We also thank Dipl.-Biol. Beate Wiebeck for evaluating the morphological characterization results. Open Access funding enabled and organized by Projekt DEAL.

Conflict of Interest

The authors declare no conflict of interest.

Data Availability Statement

The data that support the findings of this study are available in the Supporting Information of this article.

Keywords: antiproliferative agents · apoptosis · cell cycle · spirooxindoles · heterocycles

- [1] Reviews: a) L. Zhong, Y. Li, L. Xiong, W. Wang, M. Wu, T. Yuan, W. Yang, C. Tian, Z. Miao, T. Wang, S. Yang, *Signal Transduct. Target. Ther.* **2021**, *6*, 201; b) G. Sun, D. Rong, Z. Li, G. Sun, F. Wu, X. Li, H. Cao, Y. Cheng, W. Tang, Y. Sun, *Front. Cell Dev. Biol.* **2021**, *9*, 694363; c) P. L. Bedard, D. M. Hyman, M. S. Davids, L. L. Siu, *Lancet* **2020**, *395*, 1078–1088.
- [2] T. Asano, *J. Nippon Med. Sch.* **2020**, *87*, 244–251.
- [3] R. Salgia, P. Kulkarni, *Trends Cancer* **2018**, *4*, 110–118.
- [4] Reviews: a) É. Frank, G. Szöllösi, *Molecules* **2021**, *26*, 4617; b) D. K. Lang, R. Kaur, R. Arora, B. Saini, S. Arora, *Anti-Cancer Agents Med. Chem.* **2020**, *20*, 2150–2168; c) D. Kumar, S. K. Jain, *Curr. Med. Chem.* **2016**, *23*, 4338–

4394. Selected examples: d) J. T. Schille, I. Nolte, E.-M. Packeiser, L. Wiesner, J. I. Hein, F. Weiner, X.-F. Wu, M. Beller, C. Junghans, H. Murua Escobar, *Int. J. Mol. Sci.* **2019**, *20*, 5567; e) C. Roof, J.-N. Salewski, A. Stein, A. Richter, C. Maletzki, A. Sekora, H. Murua Escobar, X.-F. Wu, M. Beller, C. Junghans, *Biomol. Ther.* **2019**, *27*, 492–501; f) W. Liu, J. Beck, L. C. Schmidt, C. Roof, C. A. Pews-Davtyan, B. C. Rütgen, S. Hammer, S. Willenbrock, A. Sekora, A. Rolfs, M. Beller, B. Brenig, I. Nolte, C. Junghans, E. Schütz, H. Murua Escobar, *Oncotarget* **2016**, *7*, 35379–35389.
- [5] a) X. Wei, R. Guo, X. Wang, J.-J. Liang, H.-F. Yu, C.-F. Ding, T.-T. Feng, L.-Y. Zhang, X. Liu, X.-Y. Hu, Y. Zhou, *Molecules* **2021**, *26*, 7457; b) C.-L. Lee, C.-M. Wang, H.-C. Hu, H.-R. Yen, Y.-C. Song, S.-J. Yu, C.-J. Chen, W.-C. Li, Y.-C. Wu, *Phytochemistry* **2019**, *162*, 39–46; c) H. A. Hamid, A. N. M. Ramli, M. M. Yusoff, *Front. Pharmacol.* **2017**, *8*, 96; d) S. Sugimoto, M. Naganuma, T. Kanai, *J. Gastroenterol.* **2016**, *51*, 853–861; e) A. S. Nugraha, P. A. Keller, *Nat. Prod. Commun.* **2011**, *6*, 1953–1966; f) K. Watanabe, S. Yano, S. Horie, L. T. Yamamoto, H. Takayama, N. Aimi, S.-I. Sarai, D. Ponglux, P. Tongroach, J. Shan, P. K. T. Pang in *Pharmacological Research on Traditional Herbal Medicines, 1st Ed.*, H. Watanabe, T. Shibuya, Eds.; CRC Press, London **1999**, pp.163–178.
- [6] a) B. Yu, D.-Q. Yu, H.-M. Liu, *Eur. J. Med. Chem.* **2015**, *97*, 673–698; b) R. Ahmad, F. Salim in *Studies in Natural Product Chemistry*, Vol. 45, A.-u.-Rahman, Ed.; Elsevier, Amsterdam **2015**, pp. 485–525; c) G. A. Cordell, *Introduction to Alkaloids. A Biogenetic Approach*. Wiley-Interscience, New York **1981**, pp. 656–690.
- [7] a) M. Kaur, M. Singh, N. Chadha, O. Silakari, *Eur. J. Med. Chem.* **2016**, *123*, 858–894; b) P. Saraswat, G. Jeybalan, M. Z. Hassan, M. U. Rahman, N. K. Nyola, *Synth. Commun.* **2016**, *46*, 1643–1664; c) X.-H. Zhong, L. Xiao, Q. Wang, B.-J. Zhang, M.-F. Bao, X.-H. Cai, L. Peng, *Phytochem. Lett.* **2014**, *10*, 55–59; d) Y.-J. Wu in *Top. Heterocyclic Chem.*, Vol. 26, Heterocyclic scaffolds II: reactions and applications of indoles; G. W. Gribble, Ed.; Springer, Berlin **2010**, pp. 1–29; e) S. Peddibhotla, *Curr. Bioactive Comp.* **2009**, *5*, 20–38.
- [8] E. García Prado, M. D. García Gimenez, R. De la Puerta Vázquez, J. L. Espartero Sánchez, M. T. Sáenz Rodríguez, *Phytochemistry* **2007**, *14*, 280–284.
- [9] Y. Zhao, S. Yu, W. Sun, L. Liu, J. Lu, D. McEachern, S. Shargary, D. Bernard, X. Li, T. Zhao, P. Zou, D. Sun, S. Wang, *J. Med. Chem.* **2013**, *56*, 5553–5561.
- [10] X.-F. Cao, J.-S. Wang, X.-B. Wang, J. Luo, H.-Y. Wang, L.-Y. Kong, *Phytochemistry* **2013**, *96*, 389–396.
- [11] J.-H. Liang, Z.-L. Luan, X.-G. Tian, W.-Y. Zhao, Y.-L. Wang, C.-P. Sun, X.-K. Huo, S. Deng, B.-J. Zhang, Z.-J. Zhang, X.-C. Ma, *J. Nat. Prod.* **2019**, *82*, 3302–3310.
- [12] L. Fan, X.-J. Huang, C.-L. Fan, G.-Q. Li, Z.-L. Wu, S.-G. Li, Z.-D. He, Y. Wang, W.-C. Ye, *Nat. Prod. Commun.* **2015**, *10*, 2087–2090.
- [13] M. Kitajima, S. Ohara, Noriyuki Kogure, Y. Wu, R. Zhang, H. Takayama, *Heterocycles* **2012**, *85*, 1949–1959.
- [14] T. von Drathen, F. Hoffmann, M. Brasholz, *Chem. Eur. J.* **2018**, *24*, 10253–10259.
- [15] For other examples of photooxidative syntheses of *N*-heterocycles, see: a) M. Frahm, T. von Drathen, L. M. Gronbach, A. Voss, F. Lorenz, J. Bresien, A. Villinger, F. Hoffmann, M. Brasholz, *Angew. Chem. Int. Ed.* **2020**, *59*, 12450–12454; *Angew. Chem.* **2020**, *132*, 12550–12554; b) E. Schendera, A. Villinger, M. Brasholz, *Org. Biomol. Chem.* **2020**, *18*, 6912–6915; c) E. Schendera, L.-N. Unkel, H. Q. Phung Phan, G. Salkewitz, F. Hoffmann, A. Villinger, M. Brasholz, *Chem. Eur. J.* **2020**, *26*, 269–274.
- [16] A. Zapf, A. Ehrentraut, M. Beller, *Angew. Chem. Int. Ed.* **2000**, *39*, 4153–4155; *Angew. Chem.* **2000**, *112*, 4315–4317.

Manuscript received: March 28, 2022

Revised manuscript received: April 26, 2022

Accepted manuscript online: May 1, 2022

Version of record online: May 23, 2022